Comput. Methods Appl. Mech. Engrg. 199 (2010) 755–765

Contents lists available at ScienceDirect

Comput. Methods Appl. Mech. Engrg.

journal homepage: www.elsevier.com/locate/cma

A finite element framework for continua with boundary energies. Part II: The three-dimensional case

A. Javili, P. Steinmann *

Lehrstuhl für Technische Mechanik, Universität Erlangen-Nürnberg, Egerlandstraße 5, D-91058 Erlangen, Germany

ARTICLE INFO

Article history:
Received 22 April 2009
Received in revised form 3 November 2009
Accepted 5 November 2009
Available online 11 November 2009

Keywords:
Boundary potentials
Surface tension

ABSTRACT

This paper, in line with part I [53], is concerned with the finite element implementation of boundary potential energies and the study of their impact on the deformations of solids thereby the main thrust is the fully three-dimensional formulation and implementation incorporating anisotropic effects. Boundary effects can play a dominant role in the material behavior, the most prominent example being surface tension. However, the common modelling in continuum mechanics takes exclusively the bulk into account, nevertheless, neglecting possible contributions from the boundary. Within this contribution the boundary potentials are allowed, in general, to depend not only on the boundary deformation but also on the boundary deformation gradient and the spatial boundary normal. For the formulation of the finite element method, the concept of convected curvilinear coordinates attached to the boundary is employed and the corresponding derivations completely based on a tensorial representation are carried out. Afterwards, the discretization of the generalized weak formulation, including boundary potentials, is performed and eventually numerical examples are presented to demonstrate the boundary effects due to different proposed material models. In contrast to the previous literature on this topic, the current manuscript covers jointly the following issues related to boundary energies: (1) the formulation and implementation represents a fully three-dimensional framework at large deformations, (2) the formulation of the problem and the proposed material models are based on finite strains, however, it is shown that the linearization would lead to the small strain models proposed previously in the literature and (3) the current manuscript covers the issue of anisotropy effects on the boundary energies which to the best of our knowledge has not been exemplified earlier.

1. Introduction

Surfaces of bodies and interfaces between pairs of bodies, in general, exhibit properties different from those associated with the bulk. This behavior is caused either by the fact that the boundary of the material is exposed to e.g. oxidation, aging, coating, etc., thus obviously resulting in distinctively different properties in comparatively thin boundary layers or due to the fact that the atomic bonds are broken at the surface of the body. These effects could phenomenologically be modelled in terms of boundaries equipped with their own potential energy and it has been well studied in the literature since the milestone work by Gibbs [1] and elaborated by others, e.g. [3,18,33,34]. Such phenomena is usually modelled in terms of surface tension. The notion of a scalar valued surface tension can be generalized to surface stress of tensorial nature, see e.g. [5,44]. Note that in this manuscript the term surface is used rather than interface, since we model a body wrapped by its own surface.

From the physical point of view, it must be noted that the term "surface tension" is a mechanical quantity and can be understood as a force governed by the laws of dynamics, however, the term "surface energy" is the energy term subjected to the laws of thermodynamics. This fact is elaborated in detail in [47], see also [7,8]. The term surface energy is usually accepted as an excess energy term since a surface can be interpreted as a layer to which a certain energy is attached [32,47]. The surface energy can also be understood as a superficial energy term due to the rearrangement of atoms very near to a surface (see e.g. [23,47]). Also, it is well accepted that on the surface of a liquid a certain surface stress acts in a spherically symmetric configuration. In this manuscript the scalar value of the spherically symmetric stress is referred to as surface tension which indeed is equal to the surface energy in case of liquids. From the theoretical point of view a substantial body of literature can be found on the surface tension and surface energy, see e.g. [20,21,29,40,47] and references therein.

The numerical simulation of the surface of the body has been studied extensively when the bulk behaves like a fluid, e.g. [19,26,28,37] and also, with the variational formulation in [15,38,39].

* Corresponding author.
E-mail addresses: ali.javili@ltm.uni-erlangen.de (A. Javili), paul.steinmann@ltm.uni-erlangen.de (P. Steinmann).

0045-7825/$ - see front matter © 2009 Elsevier B.V. All rights reserved.
doi:10.1016/j.cma.2009.11.003

The elastic effects of solid surfaces, in general, have been studied, e.g. in [5,17,31] and references therein. Moreover, due to the size-dependent elastic properties of nanomaterials several manuscripts have appeared recently in the literature. Those works can be divided into two groups based on the approach that they employ. The first approach begins with the surface elastic formulation of Gurtin and Murdoch [5] and modifies the numerical framework, see [25,42,52,55]. In contrast, the second approach revolves around formulation of the total potential energy so as to capture the surface effects, see [43,50,49] and also for nanowires [45,51,54].

A systematic treatment of the boundary surface and its coupling with the bulk based on potentials as implemented here was proposed in [48] and implemented in two-dimensional case in [53]. In this respect different behaviors for the surface of the continuum body can be considered by defining the respective surface potential energy which provides the possibility to model a wide variety of the materials, including fluids. Therefore, this methodology is similar to the latter approach introduced above. Next, the surface of the body resembles a membrane coupled with the bulk and possessing the surface elastic properties of Gurtin and Murdoch [5] which follows the methodology of the first approach. In brief, this contribution can be understood as a bridge between the two approaches aforementioned above. On top of the subtle differences between the approach of this manuscript and the previous literature, it must be noted that this contribution is based on the finite strain setting incorporating anisotropies on the surface.

In this contribution, in order to determine the behavior of the surface, different material models are considered. The surface tension effect can result in numerical instabilities if the geometry of the problem is not properly chosen and therefore, a methodology to get around this problem is proposed.

This paper is organized as follows: In Section 2, the geometry and kinematics of boundaries is briefly outlined in order to introduce the notations employed in the manuscript and the Dirichlet principle of minimum potential energy including the additional contributions from the boundary is reviewed. A detailed description of the outlined definitions in Section 2 can be found in [48]. The key contribution of the paper is elaborated in Sections 3 and 4. In Section 3, the discretized form of the weak balance equations is given together with the finite element implementation procedure. Subsequently, in Section 4 different boundary material models are considered together with the derivations of their corresponding boundary Piola stress tensors and elasticity tensors which is needed for the employed Newton–Raphson scheme. Eventually, the performance of the proposed scheme is demonstrated in Section 5 by means of numerical examples.

2. Kinematics and energies of continua with boundaries

Consider a continuum body, illustrated in Fig. 1, that takes the material configuration $\mathscr{B}_0$ at time $t = 0$ and the spatial configuration $\mathscr{B}_t$ at time $t > 0$. The placement $\boldsymbol{x}$ and $\boldsymbol{X}$, respectively, in the spatial and the material configurations, are related by the invertible (nonlinear) deformation map

$$\boldsymbol{x} = \boldsymbol{\varphi}(\boldsymbol{X}). \tag{1}$$

The associated deformation gradient or rather (invertible) linear tangent map between material and spatial line elements $\mathrm{d}\boldsymbol{x} \in T\mathscr{B}_t$ and $\mathrm{d}\boldsymbol{X} \in T\mathscr{B}_0$ is defined as

$$\boldsymbol{F} := \operatorname{Grad} \boldsymbol{\varphi}(\boldsymbol{X}). \tag{2}$$

The boundary of the continuum body is described or rather covered by a two-dimensional surface in the three-dimensional embedding Euclidean space defined by

$$\mathscr{S}_0 = \partial\mathscr{B}_0 \quad \text{and} \quad \mathscr{S}_t = \partial\mathscr{B}_t. \tag{3}$$

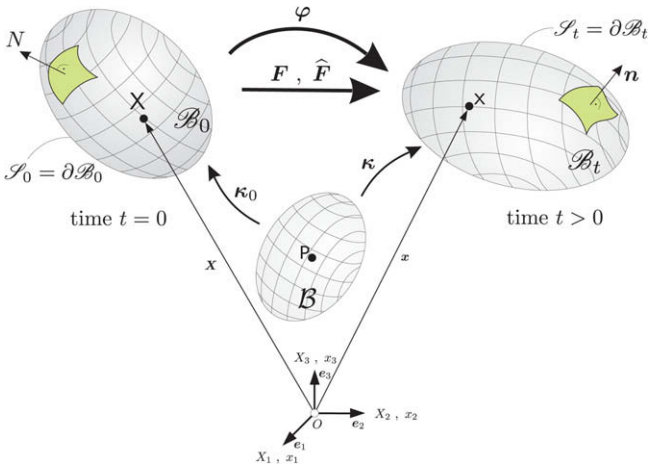

Fig. 1. Material and spatial configuration of a continuum body.

The surface deformation gradient $\widehat{\boldsymbol{F}}$ or rather (non-invertible) linear surface tangent map between line elements $\mathrm{d}\boldsymbol{X} \in T\mathscr{S}_0$ and $\mathrm{d}\boldsymbol{x} \in T\mathscr{S}_t$ is defined as

$$\widehat{\boldsymbol{F}} := \widehat{\operatorname{Grad}}\, \boldsymbol{\varphi}(\boldsymbol{X}) = \operatorname{Grad} \boldsymbol{\varphi}(\boldsymbol{X}) \cdot \widehat{\boldsymbol{I}}, \tag{4}$$

where the $\widehat{\boldsymbol{I}} := \boldsymbol{I} - \boldsymbol{N} \otimes \boldsymbol{N}$ denotes the mixed-variant surface unit tensor in the material configuration.

We define surface area elements $\mathrm{d}A$ and $\mathrm{d}a$ of $\mathscr{S}_0$ and $\mathscr{S}_t$ to be mapped into each other by the surface Jacobian $\widehat{J}$, i.e. $\mathrm{d}a = \widehat{J}\mathrm{d}A$ with $\widehat{J} := \widehat{\det}\widehat{\boldsymbol{F}}$ where the surface determinant of the surface deformation gradient is defined in accordance with Gurtin and Struthers [9] and Steinmann [48].

The total potential energy functional $I = I(\boldsymbol{\varphi})$ that we seek to minimize with respect to all admissible variations $\delta\boldsymbol{\varphi}$ (spatial variations at fixed material placement) reads

$$I(\boldsymbol{\varphi}) := \int_{\mathscr{B}_0} U_0(\boldsymbol{\varphi}, \boldsymbol{F}; \boldsymbol{X})\, \mathrm{d}V + \int_{\mathscr{S}_0} \mathrm{u}_0(\boldsymbol{\varphi}, \boldsymbol{n}, \widehat{\boldsymbol{F}}; \boldsymbol{X}, \boldsymbol{N})\, \mathrm{d}A \tag{5}$$

in which U_0 denotes the bulk potential energy density per material unit volume in $\mathscr{B}_0$ composed of internal and external contributions and likewise u_0 represents the surface potential energy density per material unit area in $\mathscr{S}_0$ consisting of internal and external contributions.

Remark. Suited constitutive laws can only be found from atomistic modelling. In the overview paper by Fischer et al. [47] and in the work by Haiss [27] some information on the construction of such constitutive laws can be found. Moreover, a multiscale surface Helmholtz free energy can be constructed through the deployment of the surface Cauchy–Born hypothesis which is elaborated in [43,45,49,50].

The minimization of the total potential energy functional, $\delta I(\boldsymbol{\varphi}) = 0$, renders the principle of virtual work including contributions from boundary terms

$$\begin{aligned} &\int_{\mathscr{B}_0} \boldsymbol{P} : \operatorname{Grad} \delta\boldsymbol{\varphi}\, \mathrm{d}V + \int_{\mathscr{S}_0} \widehat{\boldsymbol{P}} : \widehat{\operatorname{Grad}}\, \delta\boldsymbol{\varphi}\, \mathrm{d}A + \int_{\mathscr{S}_0} [\boldsymbol{n} \otimes \widehat{\boldsymbol{S}}_0] : \widehat{\operatorname{Grad}}\, \delta\boldsymbol{\varphi}\, \mathrm{d}A \\ &\quad = \int_{\mathscr{B}_0} \boldsymbol{b}_0 \cdot \delta\boldsymbol{\varphi}\, \mathrm{d}V + \int_{\mathscr{S}_0} \hat{\boldsymbol{b}}_0 \cdot \delta\boldsymbol{\varphi}\, \mathrm{d}A \quad \forall \delta\boldsymbol{\varphi}. \end{aligned} \tag{6}$$

The stress in two-point description and the distributed (volume) force related to the bulk $\mathscr{B}_0$ are defined, as usual, as

$$\boldsymbol{P} := \partial_{\boldsymbol{F}} U_0 \quad \text{and} \quad \boldsymbol{b}_0 := -\partial_{\boldsymbol{\varphi}} U_0. \tag{7}$$

Likewise, the stress in two-point description and the distributed force (the surface load or rather tractions) related to the surfaces in $\mathscr{S}_0$ are defined as

$$\widehat{\boldsymbol{P}} := \partial_{\widehat{\boldsymbol{F}}} \mathrm{u}_0 \quad \text{and} \quad \hat{\boldsymbol{b}}_0 := -\partial_{\boldsymbol{\varphi}} \mathrm{u}_0. \tag{8}$$

As an additional quantity a deformational surface shear related to $\mathscr{S}_0$ is defined as

$$\widehat{\boldsymbol{S}}_0 := \hat{\pi}_t \cdot \widehat{\operatorname{cof} \boldsymbol{F}} \quad \text{with } \hat{\pi}_t := -\partial_{\boldsymbol{n}} \mathrm{u}_t \cdot \hat{\boldsymbol{i}}, \tag{9}$$

where u_t denotes the surface internal potential energy density per spatial unit area. The denomination surface shear has been introduced before in [22]. More details on this is given in [48]. Note that we recover for the special case $\mathrm{u}_0 = \mathrm{u}_0(\boldsymbol{\varphi})$ the ordinary traction equilibrium condition $\boldsymbol{P} \cdot \boldsymbol{N} = \hat{\boldsymbol{b}}_0$.

3. Finite element discretization and implementation

In order to have an efficient finite element framework, the surface elements have to be consistent with the bulk. For instance, if the bulk is discretized by means of quadratic tetrahedra, the surface elements are also quadratic. From the point of view of implementation, this choice has the advantage that the facets of the bulk element can be regarded as surface elements if they only belong to one bulk element. This fact is illustrated in Fig. 2 for quadratic tetrahedra.

The principle of virtual work achieved in (6) is discretized into a set of bulk elements and a set of surface elements with

$$\mathscr{B}_0 = \bigcup_{\beta=1}^{n_{\text{b-el}}} \mathscr{B}_0^{\beta}, \quad \mathscr{S}_0 = \bigcup_{\gamma=1}^{n_{\text{s-el}}} \mathscr{S}_0^{\gamma}, \tag{10}$$

where $n_{\text{b-el}}$ stands for the number of bulk elements and $n_{\text{s-el}}$ stands for the number of surface elements.[1]

The geometry for each surface element can be written as a function of natural coordinate ξ by using standard two-dimensional interpolations and Galerkin approximations:

$$\boldsymbol{\varphi}(\xi) \approx \sum_{i=1}^{N_{\text{node}}} \widehat{N}^i(\xi) \boldsymbol{\varphi}^i \quad \text{and} \quad \boldsymbol{X}(\xi) \approx \sum_{i=1}^{N_{\text{node}}} \widehat{N}^i(\xi) \boldsymbol{X}^i. \tag{11}$$

Here $\xi = (\xi_1, \xi_2)$ are the natural coordinates in two dimensions (see Fig. 3) and $\widehat{N}^i$ is the standard shape function of the surface element at node i.

Equipped with the above formulae, the weak form of the balance equation associated with bulk element β with attached surface elements γ for each local node i is eventually discretized into

$$\begin{aligned} \boldsymbol{R}_e^i := & \int_{\mathscr{B}_0^{\beta}} \boldsymbol{P} \cdot \operatorname{Grad} N^i \, \mathrm{d}V + \int_{\mathscr{S}_0^{\gamma}} \widehat{\boldsymbol{P}} \cdot \widehat{\operatorname{Grad}} \, \widehat{N}^i \, \mathrm{d}A \\ & + \int_{\mathscr{S}_0^{\gamma}} [\boldsymbol{n} \otimes \widehat{\boldsymbol{S}}_0] \cdot \widehat{\operatorname{Grad}} \, \widehat{N}^i \, \mathrm{d}A - \int_{\mathscr{B}_0^{\beta}} \boldsymbol{b}_0 N^i \, \mathrm{d}V - \int_{\mathscr{S}_0^{\gamma}} \hat{\boldsymbol{b}}_0 \widehat{N}^i \, \mathrm{d}A, \end{aligned} \tag{12}$$

wherein the $\boldsymbol{R}_e^i$ denotes the residual vector for a local node i and which must be set to zero. In order to solve $\boldsymbol{R}_e^i = 0$, the Newton–Raphson scheme can be utilized.

The global residual at the global node J is defined by

$$\boldsymbol{R}^J := \mathop{\mathsf{A}}_{e=1}^{n_{\text{el}}} \boldsymbol{R}_e^j, \tag{13}$$

where the corresponding local node number in an element or surface element e to the global node number J is denoted by $j = 1, n_{\text{ne}}$ and n_{ne} is the number of nodes per element or surface element. Herein the operator $\mathbf{A}_{e=1}^{n_{\text{el}}}$ denotes the assembly of all element and surface elements contributions at the global node $J = 1, n_{\text{np}}$ where n_{np} is the total number of nodes.

[1] In the current manuscript the discretization procedure for the bulk is skipped, for the sake of space. Nevertheless, a similar strategy can be used as has been introduced in the literature, e.g. [16,46].

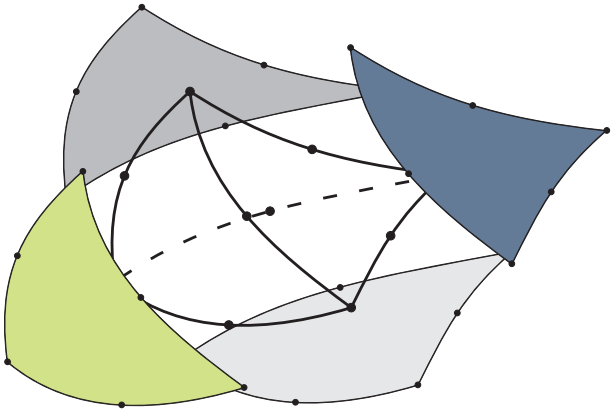

Fig. 2. Illustration of consistency of the surface elements with the bulk.

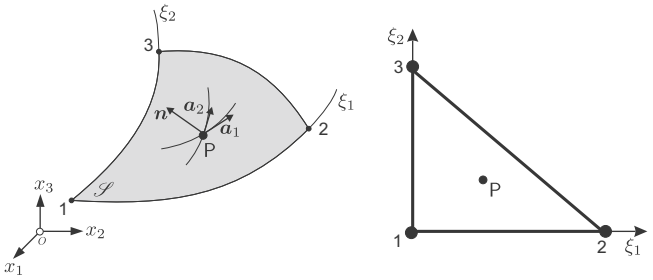

Fig. 3. Curvilinear coordinate system assigned to the two-dimensional surface element.

The consistent linearization of the resulting system of equations, would be

$$\boldsymbol{R}(\boldsymbol{d}) + \left.\frac{\partial \boldsymbol{R}}{\partial \boldsymbol{d}}\right|_n \Delta \boldsymbol{d} = \boldsymbol{0} \quad \text{and} \quad \boldsymbol{d}_{n+1} = \boldsymbol{d}_n + \Delta \boldsymbol{d}, \tag{14}$$

in which n stands for the iteration step and $\boldsymbol{R}$ and $\boldsymbol{d}$ are the global vectors of residual and spatial coordinates defined, e.g. by

$$\boldsymbol{d} = [\boldsymbol{\varphi}^1, \ldots, \boldsymbol{\varphi}^J, \ldots, \boldsymbol{\varphi}^{n_{\text{np}}}]^T, \quad \boldsymbol{R} = [\boldsymbol{R}^1, \ldots, \boldsymbol{R}^J, \ldots, \boldsymbol{R}^{n_{\text{np}}}]^T. \tag{15}$$

Solving (14) results in the spatial coordinate increment, $\Delta \boldsymbol{d}$ and consequently $\boldsymbol{d}_{n+1}$.

The local tangent stiffness would be

$$\begin{aligned} \left[\boldsymbol{K}_e^{ij}\right]_{ac} = \left[\frac{\partial \boldsymbol{R}_e^i}{\partial \boldsymbol{\varphi}^j}\right]_{ac} = & \int_{\mathscr{B}_0^{\beta}} \{\operatorname{Grad} N^i\}_b \{\mathbb{A}\}_{abcd} \{\operatorname{Grad} N^j\}_d \, \mathrm{d}V \\ & + \int_{\mathscr{S}_0^{\gamma}} \{\widehat{\operatorname{Grad}} \, \widehat{N}^i\}_b \{\widehat{\mathbb{A}}\}_{abcd} \{\widehat{\operatorname{Grad}} \, \widehat{N}^j\}_d \, \mathrm{d}A \\ & + \int_{\mathscr{S}_0^{\gamma}} \{\widehat{\operatorname{Grad}} \, \widehat{N}^i\}_b \{\widehat{\mathbb{H}}\}_{abcd} \{\widehat{\operatorname{Grad}} \, \widehat{N}^j\}_d \, \mathrm{d}A, \end{aligned} \tag{16}$$

in which $\mathbb{A}$ is the fourth-order elasticity two-point tensor as has been introduced in [13]. $\widehat{\mathbb{A}}$ and $\widehat{\mathbb{H}}$ are defined, in analogy, as follows:

$$\mathbb{A} = \frac{\partial \boldsymbol{P}}{\partial \boldsymbol{F}} \quad \text{and} \quad \widehat{\mathbb{A}} = \frac{\partial \widehat{\boldsymbol{P}}}{\partial \widehat{\boldsymbol{F}}} \quad \text{and} \quad \widehat{\mathbb{H}} = \frac{\partial [\boldsymbol{n} \otimes \widehat{\boldsymbol{S}}_0]}{\partial \widehat{\boldsymbol{F}}}. \tag{17}$$

Finally in analogy to (13), the global tangent stiffness of the whole system has to be assembled

$$\boldsymbol{K}^{IJ} = \mathop{\mathsf{A}}_{e=1}^{n_{\text{el}}} \boldsymbol{K}_e^{ij}. \tag{18}$$

It is noteworthy that the assembly operator introduced here is slightly different from that introduced in the literature, e.g. [24,35], in the sense that here the contributions from both the bulk and the boundary surface have to be taken into account.

4. Examples for boundary potentials

In order to model a specific material behavior of the boundary, first the internal potential energy of the boundary material, $\mathrm{w}_0(\widehat{\boldsymbol{F}},\boldsymbol{n};\boldsymbol{X},\boldsymbol{N})$, is defined. Next, the corresponding derivations are carried out so as to achieve the boundary Piola stress and elasticity tensor $\widehat{\boldsymbol{P}}$ and $\widehat{\mathbb{A}}$, respectively, as well as $\boldsymbol{n}\otimes\widehat{\boldsymbol{S}}_0$ and $\widehat{\mathbb{H}}$ which are contributions explicitly from the anisotropic part of the boundary energy. In this contribution two elementary options are proposed for isotropic boundary potentials in Sections 4.1 and 4.2, respectively. The first option models boundaries which behave like a neo-Hookean material and the second one models the typical surface tension. Afterwards, in Section 4.4 an anisotropic model for surface energy is proposed.

4.1. Neo-Hookean type boundary potential

For a boundary material which behaves analogously to a neo-Hookean material, however in two dimensions, so that it mimics the format e.g. advocated in [30], the internal potential energy can be expressed as

$$\mathrm{w}_0(\widehat{\boldsymbol{F}}) = \frac{1}{2}\hat{\lambda}\log^2\widehat{J} + \frac{1}{2}\hat{\mu}[\widehat{\boldsymbol{F}}:\widehat{\boldsymbol{F}} - 2 - 2\log\widehat{J}]. \tag{19}$$

The corresponding boundary Piola stress tensor takes the following explicit expression:

$$\widehat{\boldsymbol{P}} = \frac{\partial \mathrm{w}_0}{\partial \widehat{\boldsymbol{F}}} = \hat{\lambda}\log\widehat{J}\widehat{\boldsymbol{F}}^{-T} + \hat{\mu}[\widehat{\boldsymbol{F}} - \widehat{\boldsymbol{F}}^{-T}]. \tag{20}$$

Note that the push-forward of the boundary Piola stress tensor results in the boundary Cauchy stress tensor, i.e.,

$$\hat{\boldsymbol{\sigma}} = \frac{1}{\widehat{J}}\widehat{\boldsymbol{P}}\cdot\widehat{\boldsymbol{F}}^T = \hat{\lambda}\frac{\log\widehat{J}}{\widehat{J}}\hat{\boldsymbol{i}} + \hat{\mu}\frac{1}{\widehat{J}}[\hat{\boldsymbol{b}} - \hat{\boldsymbol{i}}], \tag{21}$$

where the $\hat{\boldsymbol{b}}$ denotes the left Cauchy–Green tensor on the boundary defined as $\hat{\boldsymbol{b}} = \hat{\boldsymbol{F}}\cdot\hat{\boldsymbol{F}}^T$.

Keep in mind that $\hat{\boldsymbol{\sigma}}$, here, is a surface stress rather than a surface tension that is developed in the next section. Recent researches indicate that surface tension alone is not sufficient to analyze surface effects on the mechanical behavior of nanostructures.

Moreover, the explicit representations for the fourth-order elasticity tensor $\widehat{\mathbb{A}}$ will be

$$\widehat{\mathbb{A}} = \frac{\partial\widehat{\boldsymbol{P}}}{\partial\widehat{\boldsymbol{F}}} = \hat{\lambda}\widehat{\boldsymbol{F}}^{-T}\otimes\widehat{\boldsymbol{F}}^{-T} + \hat{\mu}\widehat{\mathbb{I}} + [\hat{\lambda}\log\widehat{J} - \hat{\mu}]\widehat{\mathbb{D}}, \tag{22}$$

in which

$$\widehat{\mathbb{I}} = \frac{\partial\widehat{\boldsymbol{F}}}{\partial\widehat{\boldsymbol{F}}} = \boldsymbol{I}\overline{\otimes}\widehat{\boldsymbol{I}} \quad\text{and}\quad \widehat{\mathbb{D}} = \frac{\partial\widehat{\boldsymbol{F}}^{-T}}{\partial\widehat{\boldsymbol{F}}} = -\widehat{\boldsymbol{F}}^{-T}\underline{\otimes}\widehat{\boldsymbol{F}} + \hat{\boldsymbol{i}}^{\perp}\overline{\otimes}(\widehat{\boldsymbol{F}}\cdot\widehat{\boldsymbol{F}}^{-T}), \tag{23}$$

where

$$\{\boldsymbol{A}\overline{\otimes}\boldsymbol{B}\}_{ijkl} = A_{ik}B_{jl} \quad\text{with}\quad \{\boldsymbol{A}\underline{\otimes}\boldsymbol{B}\}_{ijkl} = A_{il}B_{jk}. \tag{24}$$

4.2. Surface tension boundary potential

The second material model for the boundary captures the surface effects in fluids, i.e. surface tension; more details can be found in [6]. For this model the potential energy per unit deformed area has to be constant due to constant surface tension on the whole boundary, see e.g. [4]. Therefore,

$$\mathrm{w}_t = \text{const.} = \hat{\gamma} \tag{25}$$

and correspondingly

$$\mathrm{w}_0(\widehat{\boldsymbol{F}}) = \hat{\gamma}\widehat{J}. \tag{26}$$

The associated boundary Piola stress tensor takes the following explicit expression:

$$\widehat{\boldsymbol{P}} = \frac{\partial \mathrm{w}_0}{\partial\widehat{\boldsymbol{F}}} = \hat{\gamma}\widehat{J}\widehat{\boldsymbol{F}}^{-T}. \tag{27}$$

The push-forward of the boundary Piola stress tensor results in the boundary Cauchy stress tensor, i.e.,

$$\hat{\boldsymbol{\sigma}} = \frac{1}{\widehat{J}}\widehat{\boldsymbol{P}}\cdot\widehat{\boldsymbol{F}}^T = \frac{1}{\widehat{J}}\hat{\gamma}\widehat{J}\widehat{\boldsymbol{F}}^{-T}\cdot\widehat{\boldsymbol{F}}^T = \hat{\gamma}\hat{\boldsymbol{i}}. \tag{28}$$

Eq. (28) is remarkable since it proves that the scalar value of the spherically symmetric surface Cauchy stress, is equal to the surface energy per unit deformed area in the current configuration, here $\hat{\gamma}$. In other words, in case of liquids the surface energy is identical to surface stress. This duality has caused a lot of confusion in the literature. Nevertheless, in this manuscript this boundary potential is named surface tension boundary potential and must not be confused with surface stress in general.

Moreover, the explicit representations for the fourth order elasticity tensor $\widehat{\mathbb{A}}$ will be

$$\widehat{\mathbb{A}} = \frac{\partial\widehat{\boldsymbol{P}}}{\partial\widehat{\boldsymbol{F}}} = \hat{\gamma}\widehat{J}[\widehat{\boldsymbol{F}}^{-T}\otimes\widehat{\boldsymbol{F}}^{-T} + \widehat{\mathbb{D}}]. \tag{29}$$

Remark. For the surface tension model one has to notice that the energy of the surface, in general, will not be minimum in the reference configuration, i.e. this model does not satisfy the growth conditions. Thus, this model has a rather unique characteristic as compared to most of the material models and hence it requires more investigations. Consequently, one has to apply the surface tension incrementally even though it is a material parameter. This approach provides a very robust algorithm in the proposed finite element framework and the excellent efficiency of that is illustrated by means of several examples, see also [53] for more details.

4.3. Generalized isotropic surface tension boundary potential

The material model proposed in Section 4.2 enforces the surface free energy per unit deformed area, w_t, to be constant on the boundary which is the typical case for fluids. However, in the general case this energy can also be dependent on the deformation of the surface. This fact is pointed out in the literature, e.g. [2,10,14]. In order to generalize the proposed model to capture such additional behavior, we assume the surface energy to be a function of the determinant of the deformation gradient similar to the work by Huang and Wang [41]. Therefore,

$$\mathrm{w}_t = \hat{\gamma}(\widehat{J}) \tag{30}$$

and correspondingly

$$\mathrm{w}_0 = \widehat{J}\hat{\gamma}(\widehat{J}). \tag{31}$$

The associated boundary Piola stress tensor takes the following explicit expression:

$$\widehat{\boldsymbol{P}} = \frac{\partial \mathrm{w}_0}{\partial \widehat{\boldsymbol{F}}} = \hat{\gamma}\widehat{J}\widehat{\boldsymbol{F}}^{-T} + \widehat{J}^2\frac{\partial \hat{\gamma}}{\partial \widehat{J}}\widehat{\boldsymbol{F}}^{-T}. \tag{32}$$

The push-forward of the boundary Piola stress tensor results in the boundary Cauchy stress tensor, i.e.,

$$\hat{\boldsymbol{\sigma}} = \frac{1}{\widehat{J}}\widehat{\boldsymbol{P}}\cdot\widehat{\boldsymbol{F}}^T = \hat{\gamma}\hat{\boldsymbol{i}} + \widehat{J}\frac{\partial \hat{\gamma}}{\partial \widehat{J}}\hat{\boldsymbol{i}}. \tag{33}$$

Of particular interest is when the current and reference configurations coincide and consequently $\widehat{J}=1$ and $\hat{\boldsymbol{i}}=\widehat{\boldsymbol{I}}$. Hence, the surface Cauchy stress tensor takes the form:

$$\hat{\boldsymbol{\sigma}}_0 = \hat{\gamma}_0\widehat{\boldsymbol{I}} \quad \text{with } \hat{\gamma}_0 = \hat{\gamma}_0^* + \hat{\gamma}_0^{**}, \tag{34}$$

where

$$\hat{\gamma}_0^* = \hat{\gamma}|_{\widehat{J}=1}, \quad \hat{\gamma}_0^{**} = \left.\frac{\partial \hat{\gamma}}{\partial \widehat{J}}\right|_{\widehat{J}=1}. \tag{35}$$

Note that the parameter $\hat{\gamma}_0^*$ represents the liquid nature of the material and in contrast, the parameters $\hat{\gamma}_0^{**}$ reflects the intrinsic behavior of (elastic) solids.

Remark. Note that the material models proposed here are not violating the definitions of surface stress given by Cammarata [14] and the linear constitutive law in [25] based on infinitesimal surface strain tensor. Moreover, the linear energy density given in [55] is indeed the same as what is proposed here in Section 4.3. However, the derivations in this work are based on finite deformations and consistencies with the previous works are not obvious. So as to show these similarities, the linearized form of the equations for a material model combined from both models in Sections 4.1 and 4.3 will be given in here. Hence, for the combined model, the internal potential energy is expressed as

$$\mathrm{w}_0(\widehat{\boldsymbol{F}}) = \frac{1}{2}\hat{\lambda}\log^2\widehat{J} + \frac{1}{2}\hat{\mu}[\widehat{\boldsymbol{F}}:\widehat{\boldsymbol{F}} - 2 - 2\log\widehat{J}] + \widehat{J}\hat{\gamma}(\widehat{J}), \tag{36}$$

and the boundary Piola stress tensor is

$$\widehat{\boldsymbol{P}} = \frac{\partial \mathrm{w}_0}{\partial \widehat{\boldsymbol{F}}} = \hat{\lambda}\log\widehat{J}\widehat{\boldsymbol{F}}^{-T} + \hat{\mu}[\widehat{\boldsymbol{F}} - \widehat{\boldsymbol{F}}^{-T}] + \hat{\gamma}\widehat{J}\widehat{\boldsymbol{F}}^{-T} + \widehat{J}^2\frac{\partial \hat{\gamma}}{\partial \widehat{J}}\widehat{\boldsymbol{F}}^{-T}. \tag{37}$$

The surface stress tensor close to the reference configuration can be computed by a linearization of the boundary Piola–Kirchhoff stress tensor at the reference configuration, i.e. $\widehat{\boldsymbol{F}}=\widehat{\boldsymbol{I}}$. For that, the boundary Piola–Kirchhoff stress tensor, $\widehat{\boldsymbol{S}}$, is computed by

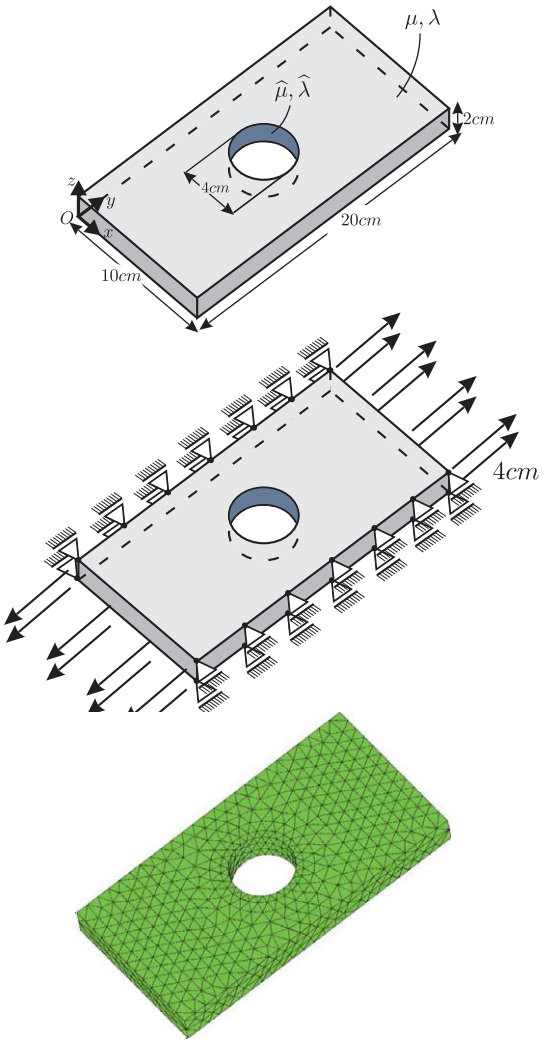

Fig. 4. Rectangular block with the hole.

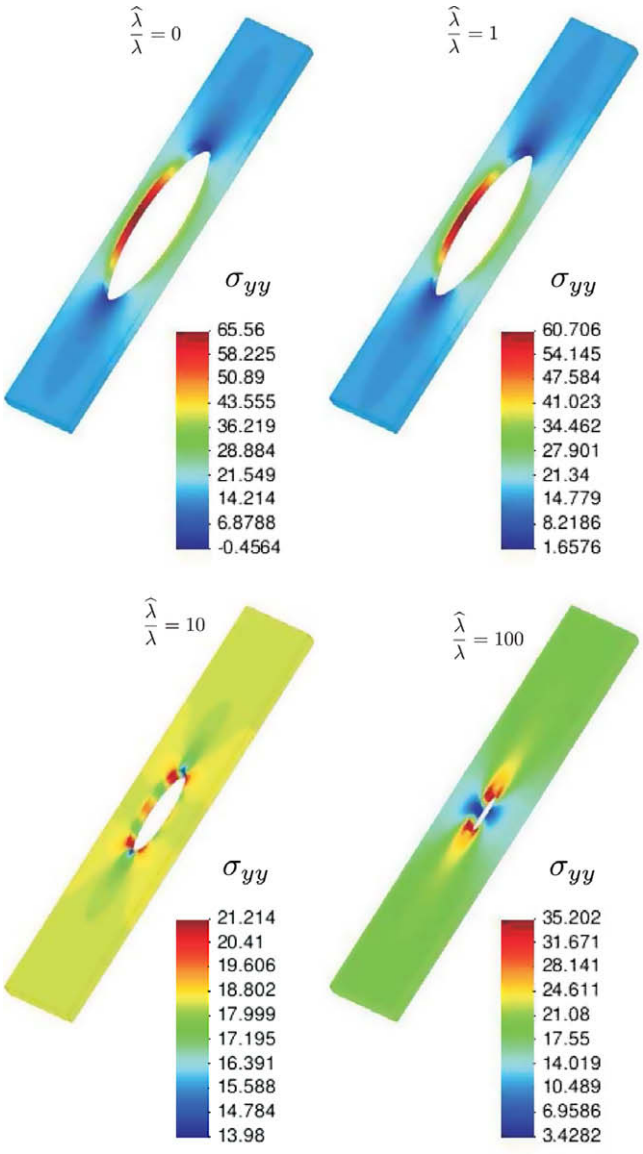

Fig. 5. Illustration of the neo-Hookean type boundary effects.

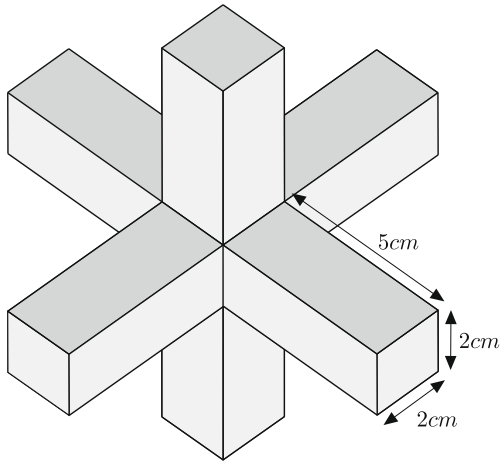

Fig. 6. A model to illustrate the surface tension boundary energies.

$$\widehat{\boldsymbol{S}} = \widehat{\boldsymbol{F}}^{-1}\cdot\widehat{\boldsymbol{P}} = \hat{\lambda}\log\widehat{J}\widehat{\boldsymbol{B}} + \hat{\mu}[\widehat{\boldsymbol{I}} - \widehat{\boldsymbol{B}}] + \hat{\gamma}\widehat{J}\widehat{\boldsymbol{B}} + \widehat{J}^2\frac{\partial\hat{\gamma}}{\partial\widehat{J}}\widehat{\boldsymbol{B}}, \tag{38}$$

where the $\widehat{\boldsymbol{B}}$ denotes the boundary Piola deformation tensor defined as $\widehat{\boldsymbol{B}} := \widehat{\boldsymbol{F}}^{-1}\cdot\widehat{\boldsymbol{F}}^{-T}$. Thus, the surface stress tensor close to the reference configuration is

$$\hat{\boldsymbol{\sigma}} = \mathrm{Lin}\,\widehat{\boldsymbol{S}}|_{\widehat{\boldsymbol{B}}=\widehat{\boldsymbol{I}}} = \widehat{\boldsymbol{S}}|_{\widehat{\boldsymbol{B}}=\widehat{\boldsymbol{I}}} + \left.\frac{\partial\widehat{\boldsymbol{S}}}{\partial\widehat{\boldsymbol{B}}}\right|_{\widehat{\boldsymbol{B}}=\widehat{\boldsymbol{I}}} : [\widehat{\boldsymbol{B}} - \widehat{\boldsymbol{I}}], \tag{39}$$

and after some mathematical steps, the constitutive relation for the surface stress tensor based on the infinitesimal surface strain tensor, denoted by $\hat{\epsilon} = \widehat{\mathrm{Grad}}^{\mathrm{sym}}\,\boldsymbol{u}$, can be derived as follows:

$$\hat{\boldsymbol{\sigma}} = \hat{\boldsymbol{\sigma}}_0 + \widehat{\mathbb{C}} : \hat{\epsilon}, \tag{40}$$

in which the $\hat{\boldsymbol{\sigma}}_0$ denotes the surface stress when the bulk is unstrained and can be calculated by Eq. (34). Also, the fourth-order constitutive tensor $\widehat{\mathbb{C}}$ can be explicitly expressed as

$$\widehat{\mathbb{C}} = \hat{\lambda}\widehat{\boldsymbol{I}}\otimes\widehat{\boldsymbol{I}} + 2\hat{\mu}\widehat{\boldsymbol{I}}\overline{\otimes}\widehat{\boldsymbol{I}} + 2\hat{\gamma}_0[\widehat{\boldsymbol{I}}\otimes\widehat{\boldsymbol{I}} + \widehat{\boldsymbol{I}}\overline{\otimes}\widehat{\boldsymbol{I}}] + \hat{\gamma}_0^*\,\widehat{\boldsymbol{I}}\overline{\otimes}\widehat{\boldsymbol{I}}, \tag{41}$$

in which

$$\hat{\gamma}_0^* := \frac{\partial}{\partial\widehat{J}}\left(\frac{\partial\hat{\gamma}}{\partial\widehat{J}}\right)\bigg|_{\widehat{J}=0}. \tag{42}$$

Furthermore, Eq. (40) can be simplified to

$$\begin{aligned}\hat{\boldsymbol{\sigma}} = {}& \hat{\gamma}_0^*\widehat{\boldsymbol{I}} + 2\hat{\gamma}_0^*[\widehat{\mathrm{Tr}}(\hat{\epsilon})\widehat{\boldsymbol{I}} + \hat{\epsilon}] + \hat{\gamma}_0^{**}\widehat{\boldsymbol{I}} + 2\hat{\gamma}_0^{**}[\widehat{\mathrm{Tr}}(\hat{\epsilon})\widehat{\boldsymbol{I}} + \hat{\epsilon}] + \hat{\gamma}_0^*\,\hat{\epsilon}\\ & + \hat{\lambda}\widehat{\mathrm{Tr}}(\hat{\epsilon})\widehat{\boldsymbol{I}} + 2\hat{\mu}\hat{\epsilon},\end{aligned} \tag{43}$$

where $\widehat{\mathrm{Tr}}(\hat{\bullet}) = \hat{\bullet} : \widehat{\boldsymbol{I}}$ computes the trace of a second order tensor at the boundary. In Eq. (43), the first line of the equation is illustrating the nature of liquids and, in contrast, the second line is playing a role only in case of solids. Also, the last two terms are representing the Hookean type resistance of the boundary which clearly are only valid for solids.

4.4. Anisotropic surface tension boundary potential

The proposed anisotropic material model for the boundary captures anisotropic surface tension. This model represents the surface tension effect but depends on the surface Jacobian and the surface normal instead of being constant all over the surface. For this model the potential energy per unit deformed area consists of a constant $\hat{\gamma}$ due to constant surface tension on the whole boundary plus an additional part as a function of the surface normal $\boldsymbol{n}$ and the surface Jacobian $\widehat{J}$. The material parameter $\hat{\alpha}$ is chosen in order to control the anisotropic contribution compared to the isotropic part. The vector $\boldsymbol{e}$ is a given unit vector characterizing a distinguished direction. Therefore,

$$\mathrm{w}_t = \hat{\gamma}[1 + \hat{\alpha}\widehat{J}[\boldsymbol{n}\cdot\boldsymbol{e}]^2], \tag{44}$$

and consequently,

$$\mathrm{w}_0 = \hat{\gamma}\widehat{J} + \hat{\alpha}\hat{\gamma}\widehat{J}^2[\boldsymbol{n}\cdot\boldsymbol{e}]^2. \tag{45}$$

The corresponding boundary Piola stress tensor takes the explicit expression:

$$\widehat{\boldsymbol{P}} = \frac{\partial\mathrm{w}_0}{\partial\widehat{\boldsymbol{F}}} = \hat{\gamma}\widehat{J}\widehat{\boldsymbol{F}}^{-T} + \hat{\alpha}\hat{\gamma}\widehat{J}^2[2[\boldsymbol{n}\cdot\boldsymbol{e}]^2\widehat{\boldsymbol{F}}^{-T} + 2[\boldsymbol{n}\cdot\boldsymbol{e}]\widehat{\boldsymbol{\Sigma}}], \tag{46}$$

where

$$\widehat{\boldsymbol{\Sigma}} = \boldsymbol{e}\cdot\frac{\partial\boldsymbol{n}}{\partial\widehat{\boldsymbol{F}}} \quad \text{with } \frac{\partial\boldsymbol{n}}{\partial\widehat{\boldsymbol{F}}} = \frac{1}{|\boldsymbol{a}_1\times\boldsymbol{a}_2|}\hat{\boldsymbol{i}}\cdot\frac{\partial(\boldsymbol{a}_1\times\boldsymbol{a}_2)}{\partial\widehat{\boldsymbol{F}}}. \tag{47}$$

Moreover, the explicit representations for the fourth order elasticity tensor, $\widehat{\mathbb{A}}$ will be

$$\begin{aligned}\widehat{\mathbb{A}} = \frac{\partial\widehat{\boldsymbol{P}}}{\partial\widehat{\boldsymbol{F}}} = {}& \hat{\gamma}\widehat{J}\widehat{\boldsymbol{F}}^{-T}\otimes\widehat{\boldsymbol{F}}^{-T} + \hat{\gamma}\widehat{J}\widehat{\mathbb{D}}\\ & + 2\hat{\alpha}\hat{\gamma}\widehat{J}^2[2[\boldsymbol{n}\cdot\boldsymbol{e}]^2\widehat{\boldsymbol{F}}^{-T} + 2[\boldsymbol{n}\cdot\boldsymbol{e}]\widehat{\boldsymbol{\Sigma}}]\otimes\widehat{\boldsymbol{F}}^{-T}\\ & + 2\hat{\alpha}\hat{\gamma}\widehat{J}^2[2[\boldsymbol{n}\cdot\boldsymbol{e}]\widehat{\boldsymbol{F}}^{-T}\otimes\widehat{\boldsymbol{\Sigma}} + [\boldsymbol{n}\cdot\boldsymbol{e}]^2\widehat{\mathbb{D}}]\\ & + 2\hat{\alpha}\hat{\gamma}\widehat{J}^2[\widehat{\boldsymbol{\Sigma}}\otimes\widehat{\boldsymbol{\Sigma}} + [\boldsymbol{n}\cdot\boldsymbol{e}]\widehat{\mathbb{K}}] \quad \text{with } \widehat{\mathbb{K}} = \frac{\partial\widehat{\boldsymbol{\Sigma}}}{\partial\widehat{\boldsymbol{F}}}.\end{aligned} \tag{48}$$

The surface shear $\widehat{\boldsymbol{S}}_0$ can be derived as

$$\widehat{\boldsymbol{S}}_0 = \hat{\boldsymbol{\pi}}_t\cdot\widehat{\mathrm{cof}}\,\widehat{\boldsymbol{F}} = \widehat{J}\hat{\boldsymbol{\pi}}_t\cdot\widehat{\boldsymbol{F}}^{-T}, \tag{49}$$

where the $\hat{\boldsymbol{\pi}}_t$ can be expressed as

$$\hat{\boldsymbol{\pi}}_t = -\partial_{\boldsymbol{n}}\mathrm{w}_t\cdot\hat{\boldsymbol{i}} = -2\hat{\gamma}\hat{\alpha}\widehat{J}[\boldsymbol{n}\cdot\boldsymbol{e}]\hat{\boldsymbol{e}} \quad \text{with } \hat{\boldsymbol{e}} = \boldsymbol{e}\cdot\hat{\boldsymbol{i}}. \tag{50}$$

Finally,

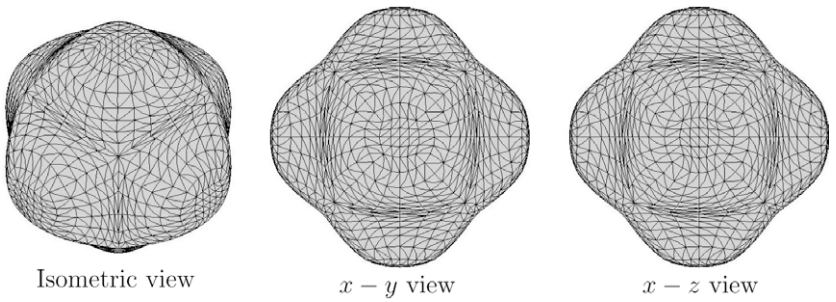

Fig. 7. Deformation of the model due to isotropic surface tension boundary energies.

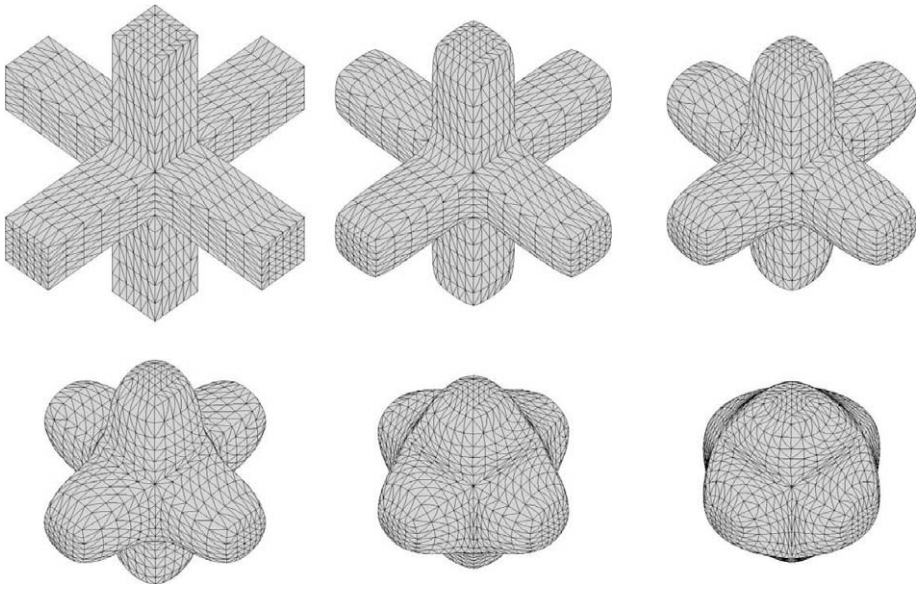

Fig. 8. Deformation of the model due to isotropic surface tension boundary energies.

$$\widehat{\mathbb{H}} = \frac{\partial(\boldsymbol{n}\otimes\widehat{\boldsymbol{S}}_0)}{\partial\widehat{\boldsymbol{F}}} = \widehat{\boldsymbol{S}}_0 \oslash \frac{\partial \boldsymbol{n}}{\partial\widehat{\boldsymbol{F}}} + \boldsymbol{n}\otimes\frac{\partial\widehat{\boldsymbol{S}}_0}{\partial\widehat{\boldsymbol{F}}}, \tag{51}$$

in which the non-standard tensor operator $\oslash$ is defined by

$$\{\boldsymbol{v}\oslash\mathscr{A}\}_{ijkl} = \mathscr{A}_{ikl}v_j. \tag{52}$$

5. Numerical examples

A number of examples in order to illustrate the effects of boundary potentials are elaborated here. For all the examples the neo-Hookean material model is assumed for the bulk with given Lamé parameters, λ and μ, as

$$W_0(\boldsymbol{F};\boldsymbol{X}) = \frac{1}{2}\lambda\log^2 J + \frac{1}{2}\mu[\boldsymbol{F}:\boldsymbol{F} - 2 - 2\log J], \quad J = \det\boldsymbol{F}. \tag{53}$$

Therefore,

$$\boldsymbol{P} = \frac{\partial W_0}{\partial\boldsymbol{F}} = [\lambda\log J - \mu]\boldsymbol{F}^{-T} + \mu\boldsymbol{F}, \tag{54}$$

and

$$\mathbb{A} = \frac{\partial\boldsymbol{P}}{\partial\boldsymbol{F}} = \lambda\boldsymbol{F}^{-T}\otimes\boldsymbol{F}^{-T} + \mu\boldsymbol{1}\overline{\otimes}\boldsymbol{1} + [\mu - \lambda\log J]\boldsymbol{F}^{-T}\underline{\otimes}\boldsymbol{F}^{-1}. \tag{55}$$

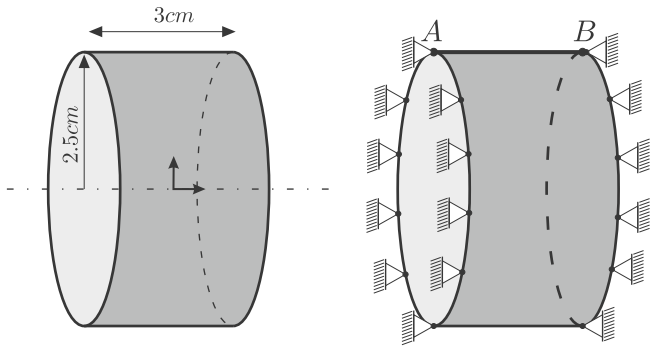

Fig. 9. A model cylinder.

The bulk is discretized by means of 10-noded tetrahedral elements and for the surface, consistent with the bulk, the 6-noded triangular elements are employed. The simulations are made by a homemade programme in C++ syntax. They run on an ordinary desktop PC within a few minutes to a few hours depending on the number of degrees of freedom.

5.1. Illustration of neo-Hookean type boundary effects

In this example a rectangular block with a hole, under prescribed displacements at end planes, i.e. $y = 0$ and $y = 20$ as shown in Fig. 4 is assumed. The lateral sides of the block, i.e. $x = 0$ and $x = 10$ are forces to have no displacement in x-direction. Respectively, the block is fixed in z-direction on the top and bottom planes, i.e. $z = 0$ and $z = 2$. The wall of the hole is subject to have surface energy of the neo-Hookean type, proposed in Section 4.1 with the material parameters $\hat{\lambda}$ and $\hat{\mu} = 0$. For the bulk, the Lamé parameters are assumed to be $\mu = 10$ MPa and $\lambda = 10$ MPa. The effects of the boundary for different values of $\hat{\lambda}$ is illustrated in Fig. 5. The model consists of 6325 nodes, 3723 quadratic tetrahedral elements and 140 quadratic triangular elements on the surface of the hole. The displacement on the lateral sides of the block, as shown in the figure, is applied in 10 equally distributed increments.

The surface material parameter $\hat{\lambda}$ tends to keep the surface area unchanged or in other words to cause $\widehat{J} = 1$ in order to minimize the surface energy. By increasing the surface material parameter $\hat{\lambda}$, or respectively the ratio $\hat{\lambda}/\lambda$, the surface energy contributions to the total energy will increase compared to that of the bulk and consequently the area of the initial (circular) hole tends to be equal to that of the final (deformed) hole which can be seen from the results shown in Fig. 5.

5.2. Illustration of isotropic surface tension effects

In order to study the effects of isotropic surface tension boundary potentials, a model as shown in Fig. 6 is considered. The isotropic surface tension potential, proposed in Section 4.2 is assigned to the surface of the model and since the initial geometry of the model is not that of the equilibrium state, the structure deforms so as to

minimize the total energy. Note that in the reference configuration the bulk energy is already minimum but it is not the case for the surface energy. The material parameters for the bulk are $\mu = 0.1$ MPa and $\lambda = 10$ MPa. The material parameter $\hat{\gamma} = 100$ N/mm is assumed for the surface. The deformed configuration is shown in Fig. 7 from different views. The model consists of 14,365 nodes, 9072 quadratic tetrahedral elements and 2160 quadratic triangular elements on the surface. The mesh quality can be observed in Fig. 8. The surface tension, $\hat{\gamma}$, is applied incrementally in 40 equal steps on the surface of the model.

The isotropic surface tension boundary potentials tends to deform the model in order to obtain the minimum surface and consequently the constant total curvature over the surface, see [48]. The deformation process towards such transformation is depicted

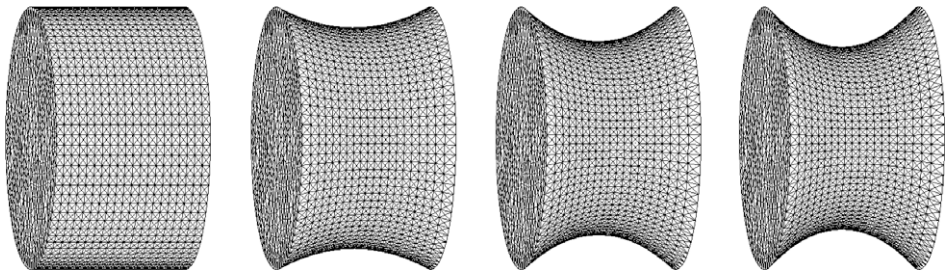

Fig. 10. Deformation of the cylinder due to the isotropic surface tension.

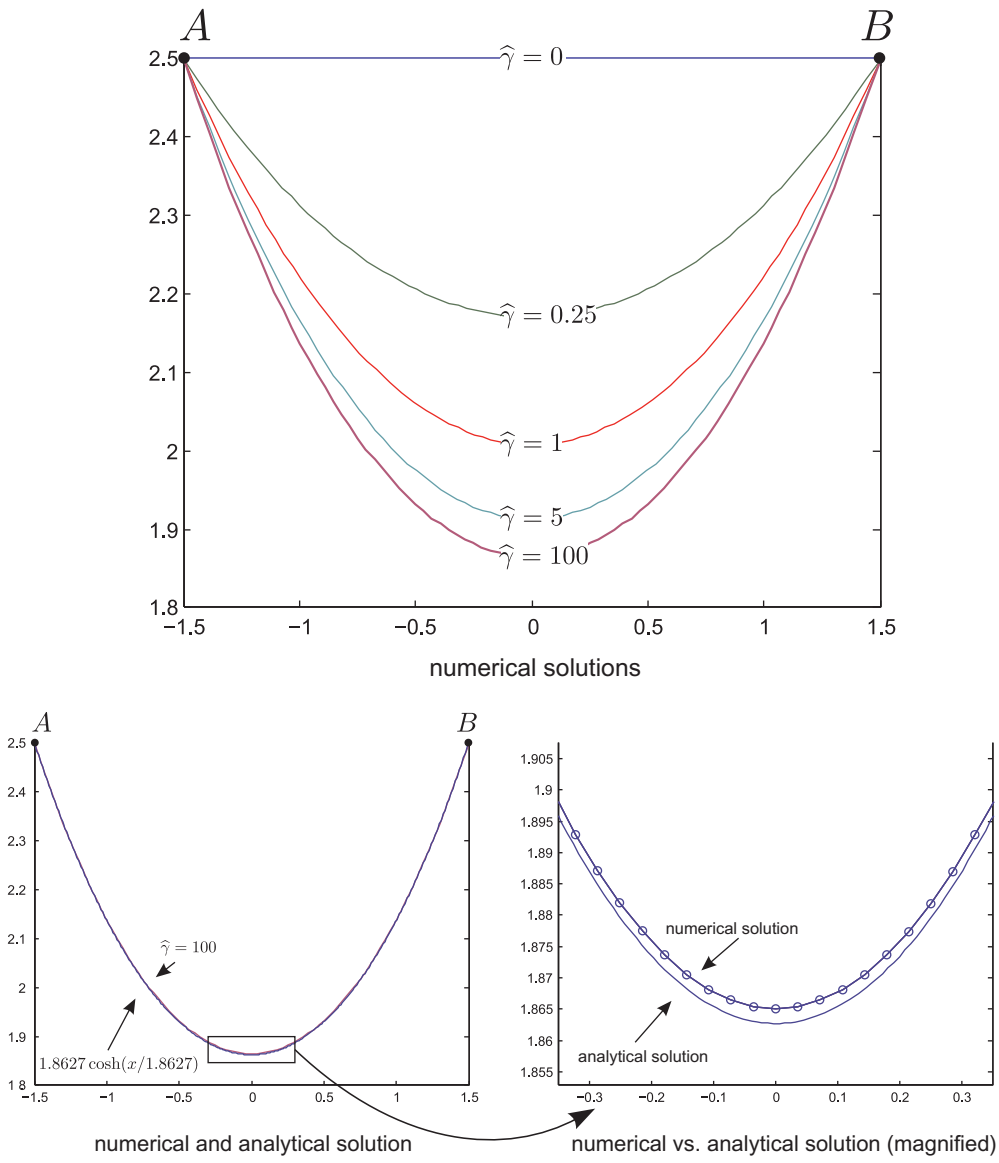

Fig. 11. Comparison of numerical and analytical results.

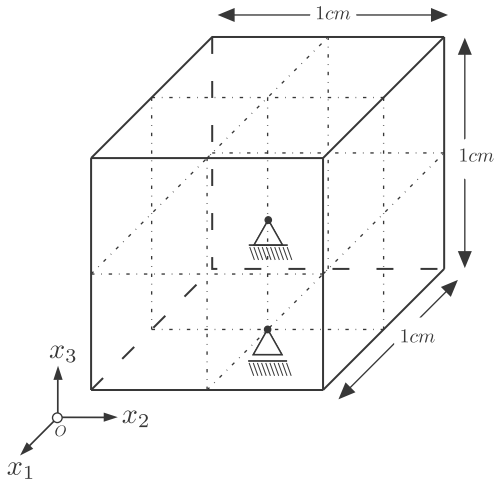

Fig. 12. A unit-cube.

in Fig. 8 at some intermediate steps. Note that the minimum surface of revolution under the isochoric deformation is a sphere, however, that is not achieved due to the fact that first the bulk is not modelled by means of an incompressible material model and second the quadratic finite elements used here are not suitable enough. Note that the problems which are driven by surface effects are very likely associated with large deformations, e.g. in fluids, and in a Lagrangian finite element framework this often leads to extremely distorted finite elements. In the worst case a mesh smoothing or even a complete remeshing becomes necessary. However we do not touch the issue of remeshing in this contribution. See also, Dettmer and Perić [37] where the authors employ the arbitrary Lagrangian–Eulerian description so as to get around this issue.

It is noteworthy that the typical convergence behavior, the norm of the residual, is quadratic and the convergence behavior of two arbitrary steps are as follows:

```
Convergence Behavior of Step 2:
1.4e+01  1.8e+00  7.3e−02  1.7e−03  1.4e−07  2.1e−11
Convergence Behavior of Step 8:
1.1e+01  7.16e−01  6.6e−02  1.9e−05  3.1e−11.
```

5.3. Liquid bridge example to illustrate the isotropic surface tension effects

This example is carried out in order to investigate deeper the isotropic surface tension effects and also to study the efficiency of the finite elements. The model is a cylinder with the dimensions shown in Fig. 9 and fixed at both ends. The isotropic surface tension boundary potentials are assigned to the surface of the model with the surface material parameter $\hat{\gamma} = 100$ N/mm. The bulk is assumed to be compressible with $\lambda = 0$ and $\mu = 0.1$ MPa. Due to the symmetry of the problem, only a quarter of the model is calculated. That consists of 20,635 nodes, 13,345 bulk element and 1600 surface elements. The surface tension is applied in 10 non-equally distributed steps.

By increasing the surface tension $\hat{\gamma}$, or respectively the ratio $\hat{\gamma}/\mu$, the model resembles more the well-known liquid bridge. In the limiting case of $\mu = 0$, the bulk would have no contribution to the energy and this example amounts to that of finding the minimum surface of revolution. The analytical solution of this problem can be attained with recourse to variational calculus, for the given dimension, as $f(x) = 1.8627\cosh(x/1.8627)$.

The process of such deformation is depicted in Fig. 10 and also the graph in Fig. 11 illustrates a set of more precise results. In this figure the deformation of the line A-B on the surface of the cylinder for different values of $\hat{\lambda}$ is shown. It can be seen that the finite element solution is approaching the analytical solution as expected. Note that the slight error can be explained by the fact that first the contribution from the bulk is not exactly zero and the shear effects are influencing the solution and also, the membrane locking effects are neglected.

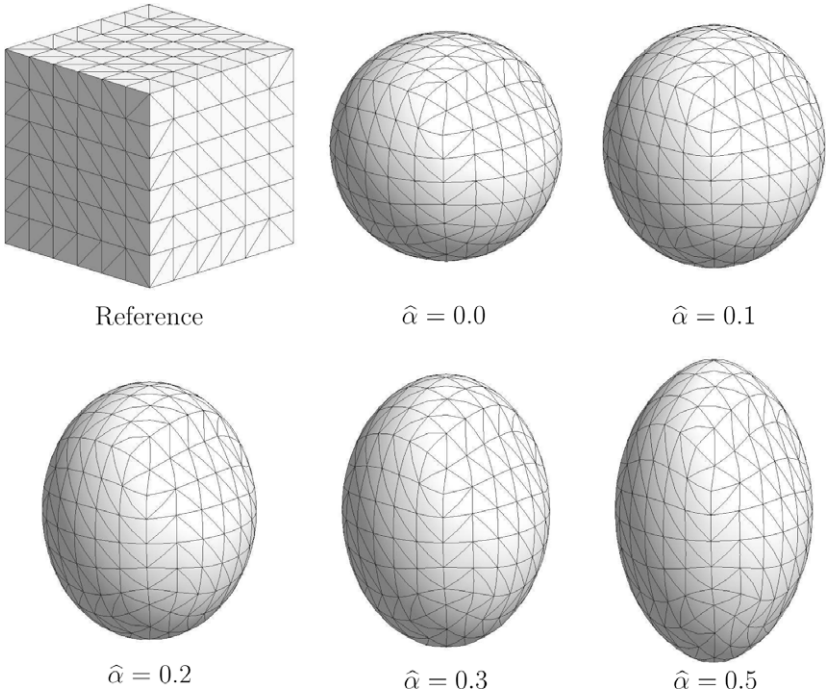

Fig. 13. Deformation of the model cube due to anisotropic surface effects.

5.4. An example to illustrate the anisotropic surface tension effects

The last example investigates the effects of anisotropic surface tension boundary potentials. To that goal, a unit-cube model as shown in Fig. 12 is considered. The model cube is fixed in translational degrees of freedom at the center and also in one additional point, taking the symmetries into account, in order to avoid the rigid body motion.

On the surface of the model the anisotropic surface tension boundary potentials, proposed in Section 4.4 is applied. Similar to the isotropic surface tension type boundary potentials, if the initial configuration does not coincide with that of the equilibrium state, the model deforms in order to minimize the total energy. Again, we note that the bulk obtains its minimum energy at the reference configuration but this is not the case for the surface. The Lamé coefficients for the bulk are $\mu = 0.1$ MPa and $\lambda = 10$ MPa and the material parameter $\hat{\gamma} = 100$ N/mm is assumed for the surface. The model consists of 2197 nodes, 1296 quadratic tetrahedral elements and 432 surface elements. The surface tension is applied in 50 increments.

For the material parameter $\hat{\alpha} = 0$ the anisotropic contribution of the surface energy vanishes and the surface tends to obtain the constant mean curvature and also to shrink. The result of such deformation would be the transformation of the model unit-cube to a sphere which can be seen in Fig. 13. By introducing the parameter $\hat{\alpha}$ the anisotropic effects can be studied. The unit vector $\boldsymbol{e} = (0, 0, 1)$ is chosen which means that the anisotropic effects will be maximum where the normal to the surface is parallel to the $\boldsymbol{e}$, i.e. on top and the bottom of the model, and will vanish where the normal to the surface is orthogonal to the $\boldsymbol{e}$, i.e. the lateral walls of the model cube. The results are shown for different values for $\hat{\alpha}$ in Fig. 13.

6. Summary

In this paper a three-dimensional finite element framework for continua with boundary potentials accounting for anisotropy has been presented. Based on geometry and kinematics of boundaries from the Dirichlet principle of minimum potential energy, the corresponding weak form of the balance equations including contributions from the boundary is derived. The discretized form of the weak form is given which provides a suitable framework for finite element implementation.

Also, in the present paper, several models for boundary potentials are introduced and various numerical examples have been provided, which confirms the excellent efficiency of the proposed scheme. The solution procedure is robust and shows the asymptotically quadratic rate of convergence for Newton–Raphson scheme.

References

[1] J.W. Gibbs, The Scientific Papers of J. Williard Gibbs, vol. 1: Thermodynamics, Longmans, Green, and Co, New York/Bombay, 1906.
[2] R. Shuttleworth, The surface tension of solids, Proc. Phys. Soc. A63 (1950) 444–447.
[3] N.K. Adam, The Physics and Chemistry of Surfaces, Oxford University Press, London, 1941.
[4] M.E. Gurtin, A continuum theory for elastic material surfaces, Arch. Rat. Mech. Anal. 112 (1975) 97–160.
[5] M.E. Gurtin, A. Murdoch, A continuum theory of elastic material surfaces, Arch. Rat. Mech. Anal. 57 (1975) 291–323.
[6] E.M. Lifshitz, L.D. Landau, Fluid Mechanics, second ed., Course of Theoretical Physics, vol. 6, Butterworth-Heinemann, 1987.
[7] P.H. Leo, R.F. Sekerka, The effect of surface stress on crystal–melt and crystal–crystal equilibrium, Acta Metall. 37 (1989) 3119–3138.
[8] P.H. Leo, R.F. Sekerka, The effect of elastic fields on the morphological stability of a precipitate grown from solid solution, Acta Metall. 37 (1989) 3139–3149.
[9] M.E. Gurtin, A. Struthers, Multiphase thermomechanics with interfacial structure. Part 3, Arch. Rat. Mech. Anal. 112 (1990) 97–160.
[10] R.J. Needs, M.J. Godfrey, M. Mansfield, Theory of surface stress and surface reconstruction, Surf. Sci. 242 (1991) 215–221.
[13] Jerrold E. Marsden, Thomas J.R. Hughes, Mathematical Foundations of Elasticity, Dover Publications, 1994.
[14] R.C. Cammarata, Surface and interface stress effects in thin films, Prog. Surf. Sci. 46 (1994) 1–38.
[15] L. Olson, E. Kock, A variational approach for modelling surface tension effects in inviscid fluids, Comput. Mech. 14 (2) (1994) 140–153.
[16] K.J. Bathe, Finite Element Procedures (Part 1–2), second ed., Prentice Hall, 1995.
[17] A.I. Rusanov, Thermodynamics of solid surfaces, Surf. Sci. Rep. 23 (1996) 173–247.
[18] W. Adamson, A.P. Gast, Physical Chemistry of Surfaces, Wiley–Interscience, 1997.
[19] S.E. Navti, K. Ravindran, C. Taylor, R.W. Lewis, Finite element modelling of surface tension effects using a Lagrangian–Eulerian kinematic description, Comput. Method Appl. Mech. Engrg. 147 (1997) 41–60.
[20] N.K. Simha, K. Bhattacharya, Equilibrium conditions at corners and edges of an interface in a multiphase solid, Mater. Sci. Engrg. A238 (1997) 32–41.
[21] N.K. Simha, K. Bhattacharya, Kinetics of phase boundaries with edges and junctions, J. Mech. Phys. Solid 46 (1998) 2323–2359.
[22] N.K. Simha, K. Bhattacharya, Kinetics of phase boundaries with edges and junctions in a three-dimensional multiphase body, J. Mech. Phys. Solid 48 (2000) 2619–2641.
[23] W.C. Johnson, Superficial stress and strain at coherent interfaces, Acta Mater. 48 (2000) 433–444.
[24] T.J.R. Hughes, The Finite Element Method: Linear Static and Dynamic Finite Element Analysis, Dover Publications, 2000.
[25] R.E. Miller, V.B. Shenoy, Size-dependent elastic properties of nanosized structural elements, Nanotechnology 11 (2000) 139–147.
[26] Michel Bellet, Implementation of surface tension with wall adhesion effects in a three-dimensional finite element model for fluid flow, Commun. Numer. Method Engrg. 17 (8) (2001) 563–579.
[27] W. Haiss, Surface stress of clean and adsorbate-covered solids, Rep. Prog. Phys. 64 (2001) 591–648.
[28] W. Dettmer, P.H. Saksono, D. Perić, On a finite element formulation for incompressible newtonian fluid flows on moving domains in the presence of surface tension, Commun. Numer. Method Engrg. 19 (9) (2003) 659–668.
[29] F.D. Fischer, NK. Simha, J. Svoboda, Kinetics of diffusional phase transformation in multicomponent elastic–plastic materials, ASME J. Eng. Mater. Technol. 125 (2003) 266–276.
[30] E. Kuhl, H. Askes, P. Steinmann, An ale formulation based on spatial and material settings of continuum mechanics. Part 1: Generic hyperelastic formulation, Comput. Method Appl. Mech. Engrg. 193 (2004) 4207–4222.
[31] P. Müller, A. Saúl, Elastic effects on surface physics, Surf. Sci. Rep. 54 (2004) 157–258.
[32] E. Fried, M.E. Gurtin, AA unified treatment of evolving interfaces accounting for small deformations and atomic transport with emphasis on grain-boundaries and epitaxy, in: H. Aref, E. Van der Giessen (Eds.), Advances in Applied Mechanics, vol. 40, 2004, pp. 1–177.
[33] G. Kaptay, Classification and general derivation of interfacial forces, acting on phases, situated in the bulk, or at the interface of other phases, J. Mater. Sci. 40 (2005) 2125–2131.
[34] P. Steinmann, O. Häsner, On material interfaces in thermomechanical solids, Arch. Appl. Mech. 75 (2005) 31–41.
[35] O.C. Zienkiewicz, R.L. Taylor, The Finite Element Method for Solid and Structural Mechanics, sixth ed., Butterworth Heinemann, 2005.
[37] W. Dettmer, D. Perić, A computational framework for free surface fluid flows accounting for surface tension, Comput. Method Appl. Mech. Engrg. 195 (23–24) (2006) 3038–3071.
[38] P.H. Saksono, D. Perić, On finite element modelling of surface tension. Variational formulation and applications. Part I: Quasistatic problems, Comput. Mech. 38 (2006) 265–281.
[39] P.H. Saksono, D. Perić, On finite element modelling of surface tension. Variational formulation and applications. Part II: Dynamic problems, Comput. Mech. 38 (2006) 251–263.
[40] F. Yang, Effect of interfacial stresses on the elastic behavior of nanocomposite materials, J. Appl. Phys. 99 (2006) 054306.
[41] Z.P. Huang, J. Wang, A theory of hyperelasticity of multi-phase media with surface/interface energy effect, Acta Mech. 182 (2006) 195–210.
[42] G. Wei, Y. Shouwen, H. Ganyun, Finite element characterization of the size-dependent mechanical behaviour in nanosystems, Nanotechnology 17 (2006) 1118–1122.
[43] H.S. Park, P.A. Klein, G.J. Wagner, A surface Cauchy–Born model for nanoscale materials, Int. J. Numer. Method Engrg. 68 (2006) 1072–1095.
[44] D. Kramer, J. Weissmüller, A note on surface stress and surface tension and their interrelation via Shuttleworth's equation and the Lippmann equation, Surf. Sci. 601 (2007) 3042–3051.
[45] H.S. Park, P.A. Klein, Surface Cauchy–Born analysis of surface stress effects on metallic nanowires, Phys. Rev. B 75 (2007). 085408-1–085408-9.
[46] J. Bonet, R.D. Wood, Nonlinear Continuum Mechanics for Finite Element Analysis, second ed., Cambridge University Press, 2008.
[47] F.D. Fischer, T. Waitz, D. Vollath, N.K. Simha, On the role of surface energy and surface stress in phase-transforming nanoparticles, Prog. Mater. Sci. 53 (2008) 481–527.
[48] P. Steinmann, On boundary potential energies in deformational and configurational mechanics, J. Mech. Phys. Solid 56 (3) (2008) 772–800.

[49] G. Yun, H.S. Park, A multiscale, finite deformation formulation for surface stress effects on the coupled thermomechanical behavior of nanomaterials, Comput. Method Appl. Mech. Engrg. 197 (2008) 3337–3350.
[50] H.S. Park, P.A. Klein, A surface Cauchy–Born model for silicon nanostructures, Comput. Method Appl. Mech. Engrg. 197 (2008) 3249–3260.
[51] J. He, C.M. Lilley, Surface effect on the elastic behavior of static bending nanowires, Nano Lett. 8 (7) (2008) 1798–1802.
[52] J. Yvonnet, H.L. Quang, Q.C. He, An XFEM/level set approach to modelling surface/interface effects and to computing the size-dependent effective properties of nanocomposites, Comput. Mech. 42 (2008) 119–131.
[53] A. Javili, P. Steinmann, A finite element framework for continua with boundary energies. Part I: The two-dimensional case, Comput. Method Appl. Mech. Engrg. 198 (2009) 2198–2208.
[54] J. He, C.M. Lilley, The finite element absolute nodal coordinate formulation incorporated with surface stress effect to model elastic bending nanowires in large deformation, Comput. Mech. 44 (2009) 395–403.
[55] H. She, B. Wang, A geometrically nonlinear finite element model of nanomaterials with consideration of surface effect, Finite Element Anal. Des. 45 (2009) 463–467.